ChemPubSoc Europe

DOI: 10.1002/chem.201904105

CHEMISTRY A European Journal Full Paper

Charge Migration

Hole Migration in Telomere-Based Oligonucleotide Anions and G-Quadruplexes

Wen Li,[a] Edita Mjekiqi,[a] Wessel Douma,[a] Xin Wang,[a] Oksana Kavatsyuk,[a, b] Ronnie Hoekstra,[a] Jean-Christophe Poully,[c] and Thomas Schlathölter*[a]

Abstract: Vacuum ultraviolet photoionization of a gas-phase oligonucleotide anion leads to the formation of a valence hole. This hole migrates towards an energetically favorable site where it can weaken bonds and ultimately lead to bond cleavage. We have studied Vacuum UV photoionization of deprotonated oligonucleotides containing the human telomere sequence dTTAGGG and G-quadruplex structures consisting of four dTGGGGT single strands, stabilized by NH_4^+ counter ions. The oligonucleotide and G-quadruplex anions were confined in a radiofrequency ion trap, interfaced with a synchrotron beamline and the photofragmentation was studied using time-of-flight mass spectrometry. Oligonucleotide 12-mers containing the 5′-TTAGGG sequence were found to predominantly break in the GGG region, whereas no selective bond cleavage region was observed for the reversed 5′-GGGATT sequence. For G-quadruplex structures, fragmentation was quenched and mostly non-dissociative single and double electron removal was observed.

Introduction

Telomeres are the protective end-caps of chromosomes in most eukaryotic organisms. In humans, a telomere typically contains about 2500 dTTAGGG repetitions at birth and this number decreases with every cell division until a critical lower limit is reached and the cell becomes senescent.[1] Telomere length is thus directly related to aging and accordingly must be maintained in highly proliferative cells such as hematopoietic stem cells. Here, the reverse transcriptase enzyme telomerase is used to add dTTAGGG sequences to the 3′ strand of chromosomes.[2] The very same enzyme is also used by 85–90% of all cancers, to keep cells in their characteristic immortal state.[3] Telomerase inhibition is thus widely considered as an attractive strategy in cancer therapy.[4,5] Telomerase dysfunction and telomere length also strongly influence the response of organisms, cells and genomes to the action of ionizing radiation.[6,7] In living cells, dTTAGGG repetitions in the single-stranded 3′ overhang can fold into stable four-stranded G-quadruplex structures with a high propensity. This typical secondary structure for instance blocks the elongating activity of telomerase. G-quadruplex stabilizing agents can therefore function as antitumor agents.[8]

In the early work of Boudaïffa et al. on DNA single and double strand break formation by resonant electron attachment to nucleobases, it is recognized that the molecular mechanisms underlying biological radiation damage can efficiently be investigated on the molecular level.[9] It is particularly straightforward to investigate the interaction of electrons, ions and photons with gas-phase DNA building blocks such as nucleobases.[10–13] Even though the relatively stable nucleobases already exhibit extensive fragmentation, gas-phase deoxyribose is even more sensitive to photon, electron or ion impact.[12,14,15] The use of neutral gas-phase targets is unfortunately not easily applicable to larger biomolecular systems such as oligonucleotides, as these systems cannot be thermally evaporated without chemical modification. Bari et al. and Milosavljevic et al. have independently developed a tandem-mass-spectrometer approach, where electrosprayed protonated peptides and proteins were accumulated in a radiofrequency ion trap and exposed to keV ions or Vacuum UV (VUV) photons before reaction products were mass analyzed.[16–18] More recently, Gonzalez-Magaña and co-workers employed this technique for the first time to investigate ionization and fragmentation of the triply protonated oligonucleotide dGCAT as induced by keV ion collisions and interactions with VUV and soft X-ray photons.[19] Mostly glycosidic bond-cleavage leading to protonated and radical nucleobase cations was observed, and it was confirmed that deoxyribose is most vulnerable. Virtually

[a] W. Li, E. Mjekiqi, W. Douma, X. Wang, Dr. O. Kavatsyuk, Prof. Dr. R. Hoekstra, Dr. T. Schlathölter
Zernike Institute for Advanced Materials, University of Groningen
Nijenborgh 4, 9747AG Groningen (The Netherlands)
E-mail: t.a.schlatholter@rug.nl

[b] Dr. O. Kavatsyuk
University College Groningen, University of Groningen
Hoendiepskade 23/24, 9718 BG Groningen (The Netherlands)

[c] Dr. J.-C. Poully
CIMAP laboratory UMR 6252
Université de Caen Normandie/CEA/CNRS/ENSICAEN
Bd Becquerel, 14070 CAEN Cedex 5 (France)

The ORCID identification number(s) for the author(s) of this article can be found under: https://doi.org/10.1002/chem.201904105.

no non-dissociative ionization was observed however, which can be attributed to the destabilizing action of the positive charge. At physiological pH, the phosphate groups in the DNA backbone are negatively charged and for an experimental investigation of biological radiation action it is thus important to study deprotonated oligonucleotides.

VUV photoabsorption in such a system induces a valence shell vacancy (hole) that can be considered as an oxidative damage. The hole in turn is known to migrate towards a site with minimum ionization energy (IE) which is typically guanine. The resulting oxidized G radical then leads to strand breakage.[20,21] The low ionization energy of G in gas-phase oligonucleotides is well-established experimentally.[22] Cauët has theoretically shown that oligonucleotide IEs decrease with G number from 8.07 eV (single G) down to 6.57 eV (GGGGGG). However, the presence of A on the 5′-side of a GGG sequence leads to an IE that is almost as low as that of GGGGGG. In particular the human telomere sequence 5′-TTAGGG is therefore expected to act as a very efficient hole trap that facilitates long-range hole migration.[23] Very recently, Rackwitz et al.[24] experimentally observed an increased cross section for low energy electron induced single strand breaks for 5′-$(TTAGGG)_2$ as compared to the intermixed sequence 5′-$(TGTGTGA)_2$. On the other hand, the absolute cross section for VUV-induced single strand break induction was found to be only weakly dependent on oligonucleotide sequence.[25]

In our present work we have experimentally studied VUV photoabsorption in multiply deprotonated gas-phase oligonucleotides containing the vertebrate telomere sequence dTTAGGG and in model G-quadruplex structures formed by 4 dTGGGGT single strands.

We have deliberately chosen relatively high VUV photon energies that allow for removal of outer as well as inner valence electrons, which are the majority of electrons in organic molecules. This situation is thus closely mimicking the direct action of ionizing radiation, although the radiation used for cancer therapy can also interact with core-level electrons. Such processes will be subject of a forthcoming study.

Results and Discussion

In a first experiment, we have studied VUV photofragmentation of the triply deprotonated telomere sequence $(dTTAGGG-3H)^{3-}$ and compared this to data obtained for the longer sequences $(dTTAGGG(CCG)_2-5H)^{5-}$ and $(dTTAGGG(CCG)_4-7H)^{7-}$. The deprotonation states were chosen such that after VUV absorption, intermediates with a comparable charge to mass ratio of 1 negative charge per 3 nucleotides ($m/z \approx 920$) were formed. Fragmentation is thus always initiated in a system of approximately equal charge to mass ratio with a single VUV induced valence hole present. Note that this range of charge states is typical for native mass spectrometry although it is much less than the one negative charge per phosphate group expected in solution at neutral pH, where counterions balance electrostatic repulsion.[26] Such counterions also allow stabilizing G-quadruplex structures: we have chosen those formed by four dTGGGGT single strands and three NH_4^+ ions (each of them stands between two G tetrads).

Figure 1 displays the results for a photon energy of 30 eV. Only the m/z range where sizeable fragmentation is observed for $(dTTAGGG-3H)^{3-}$ (top panel) is displayed. For the larger oligonucleotides, fragmentation is significantly suppressed.

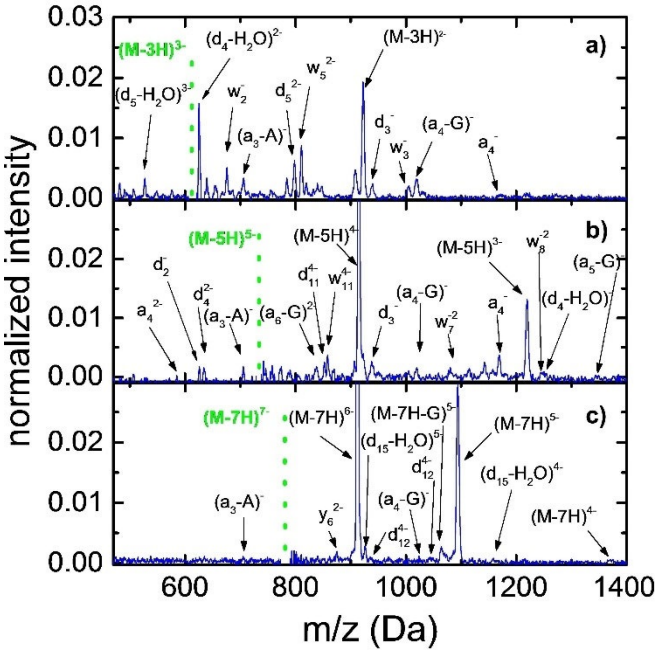

Figure 1. VUV photofragmentation spectra (30 eV) for the deprotonated oligonucleotides $(dTTAGGG-3H)^{3-}$ (a), $(dTTAGGG(CCG)_2-5H)^{5-}$ (b) and $(dTTAGGG(CCG)_4-7H)^{7-}$ (c). The spectra show the effect of the photoabsorption on the content of the RF-trap, that is, the precursor peaks (indicated by the dashed lines) are negative and not shown. All spectra are normalized to the height of the precursor peak.

Generally, the overall fragmentation probability is showing the expected decrease with size of the system: for $(dTTAGGG-3H)^{3-}$, non-dissociative electron detachment $(M-3H)^{2-}$ is of similar intensity compared to the strongest fragmentation channels, whereas for $(dTTAGGG(CCG)_2-5H)^{5-}$ non-dissociative ionization $(M-5H)^{4-}$ is about 30 times stronger than a typical fragment such as a_4^-. For $(dTTAGGG(CCG)_4-7H)^{7-}$ the respective difference amounts to 46 for the strongest $(M-7H-G)^{5-}$ fragment. The decrease in photofragmentation with the size of the system has been studied in detail for VUV photoionization of protonated peptides and can be related to an increase of heat capacity with the size of the molecule.[27] For deprotonated oligonucleotides this effect most likely is even stronger, because then fragmentation also has to compete with electron detachment. Detachment energies are known to decrease with charge state from about 5 eV for a singly deprotonated oligonucleotide[22] to less than 1 eV for $[dT_5-4H]^{4-}$.[28] This has to be compared to activation energies of the most labile bonds in deprotonated oligonucleotides, that is, glycosidic bonds with activation energies between 1 and 1.3 eV for doubly deprotonated 7-mers.[29] Danel and Parks have for instance observed autodetachment from

$(dA_7-3H)^{3-}$ on a timescale of few minutes after thermal excitation to only 102 °C.[30] The bar diagrams in Figure 2 demonstrate this effect in our data. It displays the yield of single electron removal (blue) and double electron removal (green) in

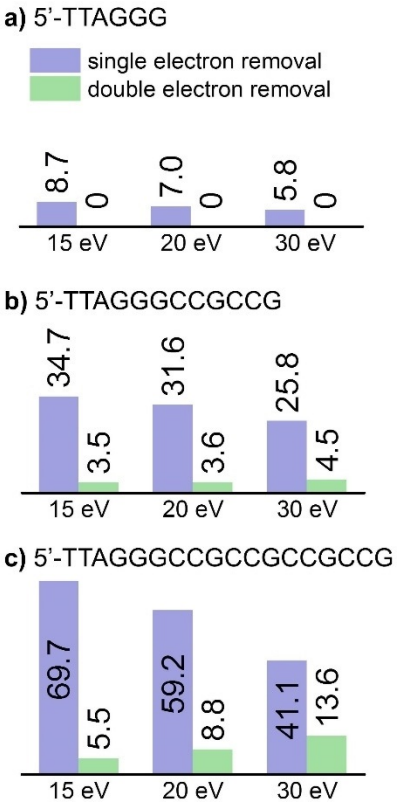

Figure 2. Single electron removal (blue) and double electron removal (green) yields in percent of the precursor ion loss for the deprotonated oligonucleotides $(dTTAGGG-3H)^{3-}$ (a), $(dTTAGGG(CCG)_2-5H)^{5-}$ (b) and $(dTTAGGG(CCG)_4-7H)^{7-}$ (c) for three photon energies.

percent of the precursor loss. Note, that the total yield of photo-ions does not need to be 100%, as detection efficiencies are smaller for large *m/z* and neutral photo-products remain unobserved. For $(dTTAGGG-3H)^{3-}$, fragmentation is dominating and for 30 eV photons, only 5.8% non-dissociative single electron removal (ND1E) is observed. This value is higher for 20 eV and 15 eV photons (7.0% and 8.7%). No ND2E is observed. For $(dTTAGGG(CCG)_2-5H)^{5-}$, fragmentation competes with ND1E (25.8% at 15 eV) and ND2E (4.5% at 15 eV). The ND1E yield increases with decreasing photon energy, whereas the ND2E yield decreases. For $(dTTAGGG(CCG)_4-7H)^{7-}$, ND1E and ND2E are dominating. ND1E decreases markedly with increasing photon energy, whereas ND2E shows the opposite trend (5.5% at 15 eV to 13.6% at 30 eV). The shift from ND1E to ND2E with increasing energy reflects the increasing probability of electron removal from low-lying valence orbitals (e.g., C, N and O 2s orbitals). The resulting inner valence vacancies can then be filled in Auger-type processes, leading to the emission of a second electron.

Most of the photofragments that can be identified from the mass spectra in Figure 1 are due to processes that involve

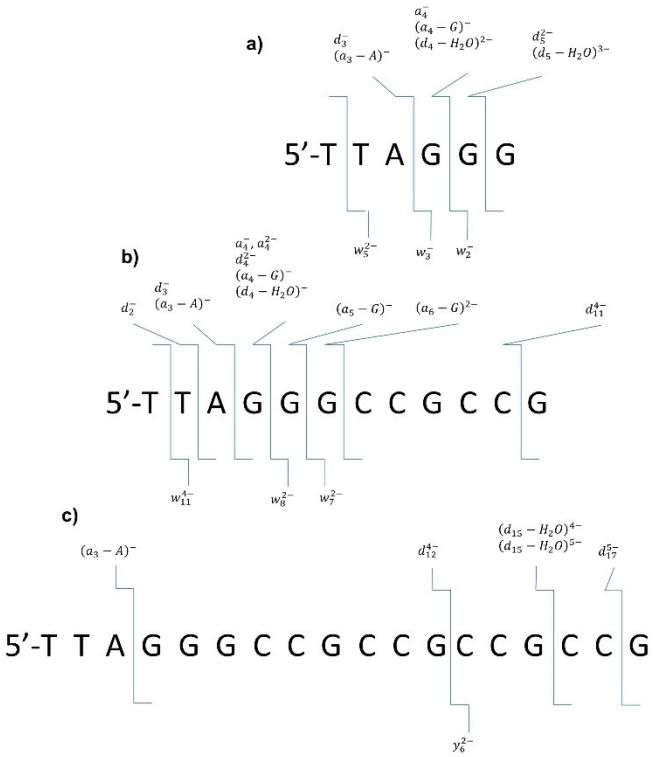

Figure 3. Fragments observed for VUV photofragmentation of $(dTTAGGG-3H)^{3-}$, $(dTTAGGG(CCG)_2-5H)^{5-}$ and $(dTTAGGG(CCG)_4-7H)^{7-}$. Fragments given above the respective sequence are from the 5′-side (left), fragments below are from the 3′-side (right).

backbone cleavage. An overview is shown in Figure 3 for the three oligomers under study. For $(dTTAGGG-3H)^{3-}$, most fragments involve backbone cleavage in the GGG region, but the entire molecule is too small and the number of fragments is too high, to draw strong conclusions from this. The situation is very different for $(dTTAGGG(CCG)_2-5H)^{5-}$. Here, photoabsorption has approximately the same probability to occur in the TTAGGG region as in the CCGCCG region but fragmentation is almost exclusively occurring in the TTAGGG part of the oligo, with a predominance in the GGG region. This finding indicates migration of the photoinduced hole towards the TTAGGG and in here mostly into the GGG region before fragmentation proceeds, as predicted by Cauët?.[23]

For $(dTTAGGG(CCG)_4-7H)^{7-}$, the strongest of the weak fragmentation channels is glycosidic bond cleavage leading to $(M-7H-G)^{5-}$ (see Figure 1). Backbone cleavage is barely observed. It mostly occurs next to G units but not predominantly in the GGG region. To summarize, the fragmentation patterns for the three oligonucleotides under study only confirm hole migration towards the GGG region for the two smallest oligonucleotides. For $(dTTAGGG(CCG)_4-7H)^{7-}$, backbone cleavage is mostly quenched by ND2E. On top of that, it is also possible that the sequence is already too long to allow for efficient hole migration.

Cauët's calculations predict that the very low vertical ionization energy and thus the high hole trapping efficiency of the telomere sequence requires the TTA to be on the 5′ side of the

GGG (vertical ionization energies: dTTAGGG: 6.76 eV, dGGGATT: 7.48 eV).[23]

Figure 4 thus shows VUV photofragmentation for $(d(GCC)_2GGGATT-5H)^{5-}$, the reverse sequence to $(dTTAGGG(CCG)_2-5H)^{5-}$. The corresponding cleavage sites are given below the spectrum. It is obvious that fragmentation is

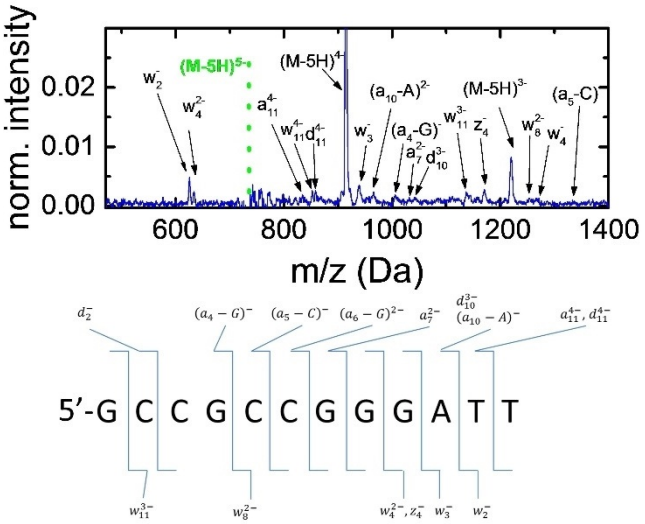

Figure 4. VUV photofragmentation spectrum (21 eV) for the sequence $(d(GCC)_2GGGATT-5H)^{5-}$. The normalization is the same as in Figure 1. The bottom Scheme indicates the observed cleavage sites.

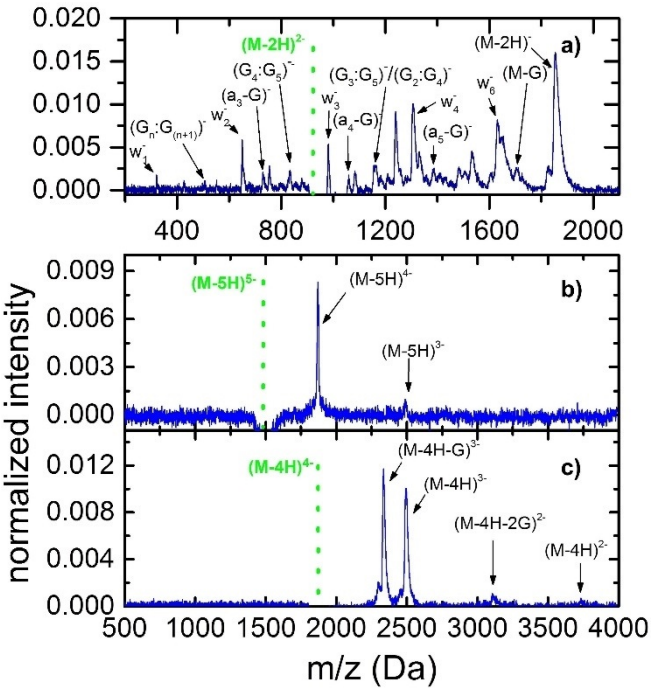

Figure 5. VUV photofragmentation spectra (21 eV) for the deprotonated oligonucleotides $(dTGGGGT-2H)^{2-}$ (a), the charge state 5− G-quadruplex structure $[(dTGGGGT)_4+3NH_4-8H]^{5-}$ formed from 4 dTGGGGT single strands and stabilized by 3 NH_4^+ counter ions (b) and the respective charge state 4− system $[(dTGGGGT)_4+3NH_4-7H]^{4-}$ (c). The normalization method is the same as in Figure 1.

much less confined to the GGG region of the oligonucleotide. Instead, backbone cleavage is distributed almost equally over the entire length of the system, in agreement with the prediction of GGG having a higher IE with an A on the 3′-side.[23]

Having confirmed the hole-trapping properties of gas-phase telomeric DNA, it is a logical next step, to study the influence of the G-quadruplex (G4) structure on VUV photoionization and photofragmentation. In their pioneering work, Gabelica et al. have used IR spectroscopy to characterize the gas-phase G4 structure.[31] In a later work they have shown that also by means of UV spectroscopy G4 structures can be assessed in the gas-phase.[32] For investigating VUV photoabsorption in a gas-phase G4, we have chosen the simplified dTGGGGT sequence which can form a tetramolecular G4 in the presence of NH_4^+ counterions.

Figure 5 (a) displays a photofragmentation spectrum obtained after absorption of one 21 eV photon by the single $(dTGGGGT-2H)^{2-}$ strand. Similar to the case of $(dTTAGGG-3H)^{3-}$ (Figure 1 a), extensive fragmentation is observed, in competition with ND1E into $(M-2H)^-$. Figure 5 (b,c) show the results for photoionization of the corresponding G4, that is, $[(dTGGGGT)_4+3NH_4-8H]^{5-}$ (b) and $[(dTGGGGT)_4+3NH_4-7H]^{4-}$ (c). The difference is striking: for the charge state 5− system, ND1E dominates and ND2E is observed as a weak feature. Clearly, the deposited energy distributes rapidly over the G4 and the size of the system is too large for fragmentation to be observed. However, for the charge state 4− G4, ND1E is accompanied by single electron removal and formation of $[(dTGGGGT)_3+(a_5\text{-}G)+2NH_4-7H]^{3-}$ that is, fragmentation of one of the four strands into a_5-G and accordingly destruction of one of the quartet structures. ND2E is observed as well and for double electron removal intense formation of $[(dTGGGGT)_2+(a_4\text{-}G)+(a_5\text{-}G)+2NH_4-7H]^{2-}$, $m/z\approx3100$], occurs, that is, fragmentation of two strands within the G4.

Photoabsorption initially only concerns one of the 4 dTGGGGT strands, constituting the G4. It is likely that the resulting electronic excitation is quickly transformed into vibrational excitation by internal conversion. UV photoexcited nucleosides are for instance undergoing non-radiative de-excitation on timescales of few ps or less.[33] Intramolecular vibrational energy redistribution (IVR) then distributes the excitation energy over the entire system. The fact that the G4 photofragmentation spectra in Figure 5 show mostly intact or modified G4s implies that IVR between the 4 dTGGGGT strands is faster than complete photofragmentation of a single strand.

The fragmentation channels seen in Figure 5 (c) are different from those observed in infrared multi-photon dissociation (IRMPD) of G4s,[31] where the underlying mechanism is a gradual increase of vibrational energy with no accompanying electron detachment. IRMPD leads to separation of the strands which subsequently dissociate into the same fragments as observed for isolated $[dTGGGGT-2H]^{2-}$. However, if single VUV induced electron removal occurs before any bond is broken, it is a radical that undergoes fragmentation. Collision-induced dissociation of radical anions formed by electron detachment from G4s has recently been found to induce extensive back-

bone fragmentation, except in regions where counterions are bound.[34] The intense fragmentation seen for $[(dTGGGGT)_4+3NH_4-7H]^{4-}$ after photodetachment may thus be due to loss of one NH_4^+ which would imply that an entire G-quartet is destabilized prior to backbone fragmentation.

The bar diagrams in Figure 6 show the yield of single electron removal (blue) and double electron removal (green) in percent of the precursor loss. For 29 eV photons, only 3.0% ND1E is observed for the G-rich monomer $(dTGGGGT-2H)^{2-}$ which increases to over 3.5% to 4.5% when photon energy

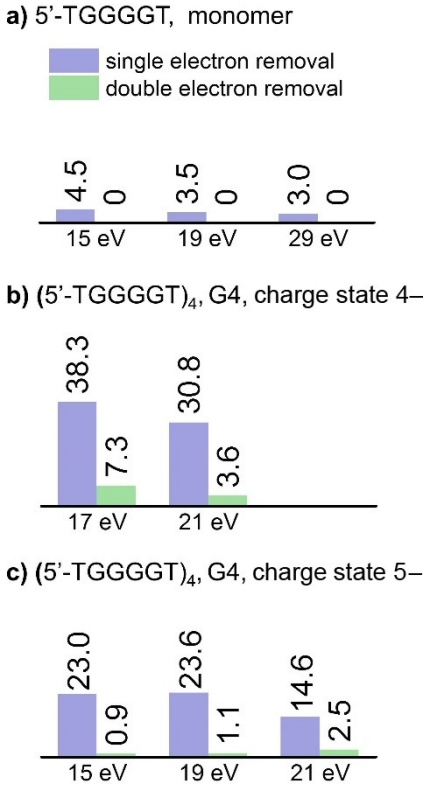

Figure 6. Single electron removal (blue) and double electron removal (green) yields for the deprotonated oligonucleotides $(dTGGGGT-2H)^{2-}$ (a), $[(dTGGGGT)_4+3NH_4-8H]^{5-}$ (b) and $[(dTGGGGT)_4+3NH_4-7H]^{4-}$ (c) for three photon energies.

decreases to 19 eV and 15 eV, respectively. ND1E is dominating the G-quadruplex spectra and decreases with photon energy for both $[(dTGGGGT)_4+3NH_4-8H]^{5-}$ (38.3% at 17 eV and 30.8% at 21 eV) and for $[(dTGGGGT)_4+3NH_4-7H]^{4-}$ (23.0% at 15 eV, 23.6% at 19 eV, 14.6% at 29 eV). On the other hand, ND2E is observed for both $[(dTGGGGT)_4+3NH_4-8H]^{5-}$ (3.6% at 21 eV) and $[(dTGGGGT)_4+3NH_4-7H]^{4-}$ (0.9% at 15 eV,1.1% at 19 eV, 2.5% at 29 eV). ND2E clearly increases with increasing photon energy which is consistent with the results obtained for the other single stranded oligonucleotides under study (see Figure 2).

Conclusions

We have investigated VUV photoabsorption in gas-phase oligonucleotide complexes which are related to human telomeric DNA. Our results confirm the notion that 5′-AGGG sequences which have a particularly low vertical ionization energy act as hole traps in gas-phase oligonucleotides ionized by VUV photoabsorption. The effect is most obvious for 12-mers, because for oligonucleotide lengths in this range, fragmentation is not overly violent as it is for smaller systems. At the same time, fragmentation is not yet quenched by electron detachment, as it is in larger oligonucleotides.

For the G-quadruplex secondary structure, which is a characteristic feature of the single stranded overhang in telomeric DNA, our data implies fast vibrational energy transfer from the initially photoionized G-rich monomer over the entire G-quadruplex structure. Fragmentation is mostly quenched and the G-quadruplexes stay intact.

Our finding confirms the notion that telomeric overhangs but also AGGG sequences within the genome are likely hotspots of oxidative damage induced by ionizing radiation. Furthermore, we are now able to study the influence of secondary structure on VUV photoinduced fragmentation processes in gas-phase experiments.

Experimental Section

The experiments presented in this work were performed using a home built tandem mass spectrometer interfaced with the U125-2 NIM VUV beamline at the BESSY II synchrotron (Helmholtz-Zentrum Berlin, Germany). The apparatus consists of an electrospray ionization (ESI) source, a radiofrequency (RF) quadrupole mass filter, a RF ion trap and a time-of-flight (TOF) mass spectrometer. It is routinely used for investigating the photophysics of biomolecular systems and has been described in detail before.[16,27]

Oligonucleotide and G-quadruplex Model System Preparation: The oligonucleotide model systems dTTAGGG (the human telomeric sequence repeat unit), $dTTAGGG(CCG)_2$, $dTTAGGG(CCG)_4$ and dTGGGGT were all purchased from LGC Biosearch technologies (Risskov, Denmark) and used without further purification. 40 μM electrospray solution consisting of 80% methanol and 20% ultrapure water (HPLC grade, Sigma–Aldrich) were made under atmospheric conditions. To facilitate G-quadruplex formation, the oligonucleotide concentration was quadrupled and 150 mM ammonium acetate (NH_4OAc) was added to the solution. The NH_4^+ ions facilitate G-quadruplex structure formation by acting as counter ions and adding charge-induced dipole interaction because they are located between G tetrads.[31]

Experimental procedure: The electrospray solutions were transferred to the ESI-emitting needle using a syringe pump with 0.8 $\mu L\,min^{-1}$ flow rate. During the ESI process, deprotonated oligonucleotides were transferred from solution into the gas phase. This process is sufficiently gentle to preserve the non-covalent bonds that stabilize G-quadruplex structures. The molecular anions passed from a heated capillary into an RF ion funnel, used for phase-space compression of the anions into a well-defined beam. The anions were then guided into the next vacuum chamber, housing an RF-octopole ion guide/trap from where bunches of ions are extracted into a quadrupole mass filter. The deprotonated oligonucleotides $(dTTAGGG-3H)^{3-}$, $(dTTAGGG(CCG)_2-5H)^{5-}$, $(dTTAGGG(CCG)_4-7H)^{7-}$ and the deprotonated G4 structures $(dTGGGGT+3NH_4-8H)^{5-}$ and $(dTGGGGT+3NH_4-7H)^{4-}$ were mass selected and subsequently enter a classical Paul trap through one of the hyperbolic end-caps. A He buffer gas pulse of 50–100 ms

duration facilitated the dissipation of the molecular ions' kinetic energy necessary for efficient ion trapping.

The setup was interfaced with the BESSY II U125-2 NIM VUV beamline. To study the radiation action, deprotonated oligonucleotide and G-quadruplex anions were exposed to the synchrotron radiation typically for a few 100 ms. Photoexposure time was controlled by means of a mechanical chopper. Eventually, photoproducts were extracted into a TOF mass spectrometer by applying a high voltage pulse to the hyperbolic end-caps of the RF-trap. A microchannel plate (MCP) detector was used to detect the photoproducts and the detector response was recorded by a 1 GHz digitizer. Typically, 500–1000 acquisition cycles were accumulated to obtain a mass spectrum with sufficient statistics.

Acknowledgements

We thank HZB for the allocation of synchrotron radiation beamtime. The research leading to this result has been supported by the project CALIPSOplus under the Grant Agreement 730872 from the EU Framework Programme for Research and Innovation HORIZON 2020. W.L. and X.W. acknowledge support by the Chinese Scholarship Council (CSC).

Conflict of interest

The authors declare no conflict of interest.

Keywords: charge migration · oligonucleotide · photoionization · synchrotron radiation · telomere

[1] L. Hayflick, *Exp. Cell Res.* **1965**, *37*, 614 – 636.
[2] P. Rousseau, C. Autexier, *RNA Biol.* **2015**, *12*, 1078 – 1082.
[3] J. W. Shay, R. R. Reddel, W. E. Wright, *Science* **2012**, *336*, 1388 – 1390.
[4] C. B. Harley, *Nat. Rev. Cancer* **2008**, *8*, 167 – 179.
[5] M. Ruden, N. Puri, *Cancer Treat. Rev.* **2013**, *39*, 444 – 456.
[6] K. Wong, S. Chang, S. Weiler, S. Ganesan, J. Chaudhuri, C. Zhu, S. Artandi, K. Rudolph, G. Gottlieb, L. Chin, F. Alt, R. DePinho, *Nat. Genet.* **2000**, *26*, 85 – 88.
[7] B. J. Sishc, C. B. Nelson, M. J. McKenna, C. L. R. Battaglia, A. Herndon, R. Idate, H. L. Liber, S. M. Bailey, *Front. Oncol.* **2015**, *5*, UNSP 257.
[8] J. Riou, L. Guittat, P. Mailliet, A. Laoui, E. Renou, O. Petitgenet, F. Megnin-Chanet, C. Helene, J. Mergny, *Proc. Natl. Acad. Sci. USA* **2002**, *99*, 2672 – 2677.
[9] B. Boudaïffa, P. Cloutier, D. Hunting, M. A. Huels, L. Sanche, *Science* **2000**, *287*, 1658.
[10] B. Coupier, B. Farizon, M. Farizon, M. J. G. F. Gobet, N. V. d. C. Faria, G. Jalbert, S. Quaskit, M. Carre, B. Gstir, G. Hanel, S. D. L. Feketova, P. Scheier, T. Märk, *Eur. Phys. J. D* **2002**, *20*, 459 – 468.
[11] J. de Vries, R. Hoekstra, R. Morgenstern, T. Schlathölter, *Phys. Rev. Lett.* **2003**, *91*, 053401.
[12] G. Hanel, B. Gstir, S. Denifl, P. Scheier, M. P. a. B. Farizon, M. Farizon, E. Illenberger, T. D. Märk, *Phys. Rev. Lett.* **2003**, *90*, 188104.
[13] H.-. Jochims, M. Schwell, H. Baumgärtel, S. Leach, *Chem. Phys.* **2005**, *314*, 263.
[14] F. Alvarado, J. Bernard, B. Li, R. Bredy, L. Chen, R. Hoekstra, S. Martin, T. Schlathölter, *ChemPhysChem* **2008**, *9*, 1254 – 1258.
[15] G. Vall-llosera, M. A. Huels, M. Coreno, A. Kivimäki, K. Jakubowska, M. Stankiewicz, E. Rachlew, *ChemPhysChem* **2008**, *9*, 1020.
[16] S. Bari, O. Gonzalez-Magaña, G. Reitsma, R. Hoekstra, J. Werner, S. Schippers, T. Schlathölter, *J. Chem. Phys.* **2011**, *134*, 024314.
[17] S. Bari, R. Hoekstra, T. Schlathölter, *Phys. Chem. Chem. Phys.* **2010**, *12*, 3376 – 3383.
[18] A. R. Milosavljević, C. Nicolas, J. Lemaire, C. Dehon, R. Thissen, J.-. Bizau, M. Refregiers, L. Nahon, A. Giuliani, *Phys. Chem. Chem. Phys.* **2011**, *13*, 15432 – 15436.
[19] O. Gonzalez-Magaña, M. Tiemens, G. Reitsma, M. Door, L. Boschmann, S. Bari, R. Hoekstra, P. O. Lahaie, M. A. Huels, R. Wagner, T. Schlathölter, *Phys. Rev. A* **2013**, *87*, 032702.
[20] T. Melvin, S. Botchway, A. Parker, P. ONeill, *J. Am. Chem. Soc.* **1996**, *118*, 10031 – 10036.
[21] C. Burrows, J. Muller, *Chem. Rev.* **1998**, *98*, 1109 – 1151.
[22] X. Yang, X. Wang, E. Vorpagel, L. Wang, *Proc. Natl. Acad. Sci. USA* **2004**, *101*, 17588 – 17592.
[23] E. Cauët, *J. Biomol. Struct. Dyn.* **2011**, *29*, 557 – 561.
[24] J. Rackwitz, I. Bald, *Chem. Eur. J.* **2018**, *24*, 4680 – 4688.
[25] S. Vogel, K. Ebel, R. M. Schuermann, C. Heck, T. Meiling, A. R. Milosavljevic, A. Giuliani, I. Bald, *ChemPhysChem* **2019**, *20*, 823 – 830.
[26] M. Porrini, F. Rosu, C. Rabin, L. Darre, H. Gomez, M. Orozco, V. Gabelica, *ACS Cent. Sci.* **2017**, *3*, 454 – 461.
[27] D. Egorov, R. Hoekstra, T. Schlathölter, *Phys. Chem. Chem. Phys.* **2017**, *19*, 20608 – 20618.
[28] J. Weber, I. Ioffe, K. Berndt, D. Loffler, J. Friedrich, O. Ehrler, A. Danell, J. Parks, M. Kappes, *J. Am. Chem. Soc.* **2004**, *126*, 8585 – 8589.
[29] J. Klassen, P. Schnier, E. Williams, *J. Am. Soc. Mass Spectrom.* **1998**, *9*, 1117 – 1124.
[30] A. Danell, J. Parks, *J. Am. Soc. Mass Spectrom.* **2003**, *14*, 1330 – 1339.
[31] V. Gabelica, F. Rosu, E. De Pauw, J. Lemaire, J. Gillet, J. Poully, F. Lecomte, G. Gregoire, J. Schermann, C. Desfrancois, *J. Am. Chem. Soc.* **2008**, *130*, 1810 – 1811.
[32] F. Rosu, V. Gabelica, E. De Pauw, R. Antoine, M. Broyer, P. Dugourd, *J. Phys. Chem. A* **2012**, *116*, 5383 – 5391.
[33] S. De Camillis, J. Miles, G. Alexander, O. Ghafur, I. D. Williams, D. Townsend, J. B. Greenwood, *Phys. Chem. Chem. Phys.* **2015**, *17*, 23643 – 23650.
[34] D. Paul, A. Marchand, D. Verga, M. Teulade-Fichou, S. Bombard, F. Rosu, V. Gabelica, *Analyst* **2019**, *144*, 3518 – 3524.

Manuscript received: September 6, 2019
Revised manuscript received: October 11, 2019
Accepted manuscript online: October 15, 2019
Version of record online: November 15, 2019

